Power System Oscillation Monitoring and Damping Control Redesign under Ambient Conditions and Multiple Operating Points

Luigi Vanfretti * **Xavier Bombois** **

* *Rensselaer Polytechnic Insitute, Troy, NY 12180 USA (e-mail: vanfrl@rpi.edu).*
** *Laboratoire Ampere, Ecole Centrale de Lyon, Universite de Lyon, Ecully, France (e-mail: xavier.bombois@ec-lyon.fr)*

Abstract: Using prediction-error identification methods, this paper proposes a measurement data-driven approach to monitor power system oscillations at a power plant, identify a data-based model using an input signal and redesign the plant's power system stabilizer damping controller to mitigate the observed oscillations under ambient conditions and multiple operating points. The advantage of the proposed methodology is that the damping performance can be monitored continuously and the redesign only requires measurements at the power plant along with the controllers structure, which are known by the power plant operator.

Keywords: Power systems, oscillation monitoring, power system stabilizer, prediction-error identification, control redesign, Bayesian optimization.

1. INTRODUCTION

Poorly damped electromechanical oscillations appear in power systems due to decreasing stability margins emerging from limited power transmission capacity, changes in the grid's operating conditions, loss of transmission corridors, etc. Such oscillations can be of local nature, i.e., resulting from the excitation of the main dynamics of a power plant connected to the reminder of the grid, or spread across "wide-areas", such as inter-area oscillations (Klein et al (1991)). A typical countermeasure to deal with such oscillations is to equip different power system apparatus with the so-called Power System Stabilizer (PSS) or Power Oscillation Dampers (POD) (Rogers (1999)). Damping control systems, i.e., PSSs and PODs, are placed preceding other control loops, such as the voltage control loop (i.e., the Excitation Control System (ECS)) in synchronous machines or voltage regulators in Static VAR Compesantors and the like (see Rebello et al (2020)). The purpose of this is to use the actuators within existing control systems to reduce oscillations and ensure the stability of the connection to the grid (in the case of a single power plant) or an entire interconnected region. However, to achieve this goal, these damping controllers should be well tuned to maintain adequate damping, and if left without calibration, may lead to major grid stability issues.

Because the structure of these controllers is fixed, the value of their parameters must be set through design studies before being implemented in the field. Existing approaches to design and tuning damping control systems largely depend on grid simulation models. However, this poses the challenge of maintaining validated models for multiple potential operating points (OPs). This is a major difficulty, especially for the European interconnected grid, as shown by recent events (ENTSO-E (2017, 2018)).

Meanwhile, the rise in the availability of power system measurements, including but not limited to Phasor Measurement Units (PMUs), allows monitoring changes in modes frequencies and damping. This ability to monitor power system dynamics can be beneficial not only for "wide-area" monitoring, but also to observe and potentially mitigate local dynamics (Mishra et al (2022)). In the previous work of the authors (see Bombois and Vanfretti (2023)) propose a data-based PSS redesign method that can be applied when the power system undergoes a disturbance (i.e. loss of a power line). In this work, we extend this approach to consider multiple operating points under ambient conditions. It should be noted that adequate damping performance is not only of interest during large system disturbances, but also as the power plant moves from one operating point (OP) to another, possibly increasing the system's stress. Power plants experience this on a regular basis, every hour, and even more frequently when they are involved in the real-time markets for energy and ancillary services. Naturally, it would be very attractive for plant owners and operators to monitor and maintain satisfactory damping performance levels at all times and in all operating conditions, which is explored in this paper.

2. PROBLEM STATEMENT AND PROPOSED METHODOLOGY

2.1 Problem Statement

To specify the problem we are trying to solve, consider the block diagram shown in Fig. 1 that represents an electrical generator of a power plant equipped with a

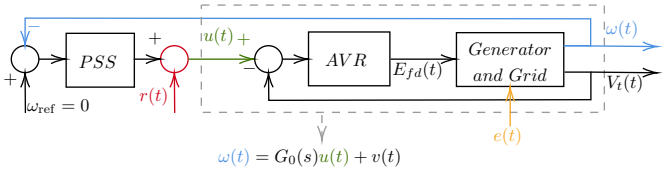

Fig. 1. Block Diagram of a Power Plant's Electrical Generator Equipped with a PSS.

PSS. Here, $\omega(t)$ is the rotor shaft speed measurement, which is used by the PSS to derive a damping signal $u(t)$, which is applied to the field control loop through the Automatic Voltage Regulator (AVR). The AVR will thus modulate $E_{fd}(t)$, the generator's field winding voltage, to damp oscillations while at the same time controlling the terminal voltage $V_t(t)$ of the generator. Note that the impact of any changes in the power grid will be reflected in $V_t(t)$ and $\omega(t)$. The signal $v(t)$ represents the influence of the random load changes $e(t)$ on $\omega(t)$. Finally, $r(t) = 0 \,\forall\, t$, except when a probing experiment is performed for identification. With this context, let us define the following linear representation of the power system (see also Fig. 1) from the point-of-view of the PSS controller:

$$\omega(t) = G_0(s)u(t) + v(t) \tag{1}$$

$$u(t) = -K(s)\omega(t) + r(t) \tag{2}$$

where $K(s)$ is the continuous-time transfer function (TF) of the PSS controller, and with $\omega(t)$, $u(t)$, $v(t)$ and $r(t)$ as defined in the preceding paragraph. In (1), $G_0(s)$ represents the dynamics of the power system between $u(t)$ and $\omega(t)$ and therefore embeds the dynamics of the AVR, generator and of the power grid to which the generator is connected. At each operating point, we can assume that these dynamics can be represented by a linear TF $G_0(s)$ (this TF will be different for each operating point). As already mentioned, the process disturbance $v(t)$ represents the effect of the random load changes on $\omega(t)$ and is here considered as filtered white noise. Using (1)-(2), we have the following expression of $\omega(t)$ in closed loop:

$$\omega(t) = T_0(s)r(t) + M_0(s)v(t), \tag{3}$$

where

$$T_0(s) = G_0(s) \;/\; \left(1 + K(s)G_0(s)\right), \tag{4}$$

$$M_0(s) = 1 \;/\; \left(1 + K(s)G_0(s)\right). \tag{5}$$

2.2 Procedure 1 — Oscillation Monitoring

Let us now discuss our monitoring and data-based control design procedures. The objective of the monitoring procedure is to evaluate the damping ability of the PSS controller. This requires to verify that all the complex poles of the closed-loop system (3) have a damping coefficient larger than a given threshold ξ_{req}. Let us for further reference denote $\xi_{min}(K, G_0)$ as the smallest value of these damping coefficients. Therefore, we wish to verify that $\xi_{min}(K, G_0) > \xi_{\text{req}}$. In what follows, we will also use an alternative notation for $\xi_{min}(K, G_0)$, i.e., $\xi_{min}(Z_0)$, where Z_0 is any closed-loop TF related to (3), e.g., T_0. If the monitoring procedure detects a drop in the performance of the PSS controller, a new PSS controller will be designed (see Procedure 3). In the monitoring procedure, we must thus determine an estimate of $\xi_{min}(K, G_0)$. For this purpose, let us first observe that, in normal operation (i.e., when $r(t) = 0$), we have that $\omega(t) = M_0(s)v(t)$ and this signal contains information on the performance of the PSS controller.

The first step in the monitoring procedure is thus to determine a time-series model of $M_0(s)v(t)$ using discrete-time data $\omega[n]$ collected in normal operation. The discrete-time sequence $\omega[n]$ can indeed be modelled as $\omega[n] = H_0(z)e[n]$ where $H_0(z)$ is a discrete-time monic, stable, inversely stable TF and $e[n]$ a white noise. Using the discrete-time data $\omega[n]$, we can then identify an Autoregressive Moving Average (ARMA) model $\hat{H}(z)$ of H_0 (and an estimate of the variance of $e[n]$). Therefore, the performance of the current PSS controller K can be assessed. For this purpose, we inspect the damping of the complex poles of $\hat{H}(z)$ and determine the minimal value of their damping, i.e., $\xi_{min}(\hat{H})$ which is an estimate of the minimal damping of the loop (1)-(2). Furthermore, we can also determine an uncertainty interval around this estimate (see Peri et al (2016) for details).

2.3 Procedure 2 — Probing-Based Identification

Next, if the estimated $\xi_{min}(\hat{H})$ (and its uncertainty interval) are deemed not satisfactory (i.e., smaller than ξ_{req}), we proceed to determine a model of G_0 in order to redesign the PSS. To this end, we excite the closed-loop system using a probing signal $r(t)$. Since G_0 may be unstable, we propose to use an indirect closed-loop approach for this purpose. Using discrete-time data $Z^N = \{r[n], \omega[n] \,|\, n = 1, , N\}$, a parametric model $\hat{T}$ of T_0 can be identified using prediction-error identification. Before proceeding to the update of the PSS controller, the model $\hat{T}$ of T_0 can be used to compute $\xi_{min}(\hat{T})$ and to verify whether a controller update is really necessary. The latter will be the case if also $\xi_{min}(\hat{T})$ is smaller than ξ_{req}. Here also, the uncertainty interval of $\xi_{min}(\hat{T})$ can be considered (see Bombois and Vanfretti (2023) for details).

2.4 Procedure 3 — PSS Redesign

If the damping is indeed insufficient we decide to update the PSS controller using a model $\hat{G}$ of G_0. Using (4), this model can be deduced from $\hat{T}$ using:

$$\hat{G}(z) = \hat{T}(z) \;/\; \left(1 - K(z)\hat{T}(z)\right) \tag{6}$$

where $K(z)$ is the discrete-time version of the current PSS controller $K(s)$. We have thus now a model $\hat{G}$ of the open-loop system G_0. With that model, we can use any control design technique to determine the new PSS controller. As an example, we can use the technique proposed in Bombois and Vanfretti (2023), which seeks to determine the PSS controller K_{new} yielding the highest value of $\xi_{min}(K_{new}, \hat{G})$ for the loop $[K_{new}\ \hat{G}]$ while satisfying H_∞ constraints that both limit the control efforts and ensure robustness.

In this paper we propose to combine the three procedures described above and apply it on a rolling basis for multiple $(k = 1, \ldots, n_{OP})$ OPs, where n_{OP} is any number of operating points, as illustrated next.

3. RESULTS

3.1 Simulation Models and Scenarios

This section starts by presenting the models and simulation scenarios used for the illustration of the proposed method in the subsequent sections.

3.1.1. Simulation Model. To illustrate the proposed methodology, we use a modified version of the classical two-area four-machine Klein-Rogers-Kundur (hereafter *KRK*) model from Klein et al (1991), implemented using the Modelica language and available from the open-source OpenIPSL library (see de Castro et al (2023)). The model is shown in Fig. 2, where the power plant of interest is shown enclosed by a red dashed square showing with a blue arrow where the input signal, $r(t)$, is applied and where data of the speed $\omega(t)$ is obtained. The simulation model includes the following component models: `GENROU` for the electrical generator `SEXS` for the AVR (see Siemens (2017)), a Type II PSS and a Type II turbine-and-governor model (see Milano (2010)); with the other plants using similar models. This model can be linearized at any point of dispatch and at any point in time, the linearization is performed according to Baur et al (2009) using the Dymola software (see Druck et al (2002)).

3.1.2. Simulation of Ambient Conditions. Recall from Fig. 1 that the power system is operating under ambient conditions, where the random variation of loads excite the grid's dynamics. To this end the model in Fig. 2 includes two inputs to excite the power system, namely $e_{Load7}(t)$ and $e_{Load9}(t)$. To model the random load variations applied to these inputs, we follow the recommendations in Klöckner et al (2017) to model a zero-mean Gaussian white noise with standard deviation of 0.025 with a 0.01 s sampling period to sample the random numbers.

3.1.3. Simulation of Multiple Operating Points. Finally, to simulate multiple OPs, i.e., different dispatch points at which the plant is operated, the required power output of the plant is varied by ramping $u_{P_m}(t)$, which is shown in the red dashed square of Fig. 2, while at the same time ramping the power demand of Load 9 using the input $e_{Load9}(t)$. These simulation scenarios are designed so that as the power dispatch (and load) are increased, the system's damping will reduce, and vice versa (see Rogers (1999)), while at the same time exciting the system's dynamics though the random loads. The ramping rates at which the plant is ramped-up/down are consistent with those of modern natural gas plants with values provided in Xu et al (2017).

A timing diagram showing how the simulation scenarios are created considering ramping to obtain new OPs, the application of $r(t)$ and the new PSS design is shown in Fig. 3. The power plant is operating at $P \approx 7.00$ per unit (p.u., 100 MVA base) at $t_A = 0$ min. and transitions to a new OP at $t_\alpha = 7.5$ min, where the proposed methodology starts being applied. As the system moves to different OPs, the power system is near an equilibrium at $t_{\alpha,\beta,\gamma,\delta,\psi} = [7.5, 25.0, 40.0, 55.0, 67.5]$ where the power dispatch is $P_{\alpha,\beta,\gamma,\delta,\psi} = [7.83, 8.29, 8.02, 7.73]$, where procedure 1 is applied. Meanwhile, procedure 2 is applied in the periods $t_{B-C} = [12.5, 17.5]$, $t_{D-E} = [27.5, 32.5]$, $t_{F-G} = [42.5, 47.5]$ and $t_{H-I} = [57.5, 62.5]$. If it is decided that the PSS redesign should be applied, i.e., if Procedure 3 is to be followed, this will take place in t_{K_x}, where $x = 0, 1, ..., 4$ and K_0 represents the original PSS.

To illustrate, in Fig. 4, results from simulating the power system as the power plant transitions between multiple OPs with a dispatch of $P_{\alpha,\beta,\gamma,\delta,\psi}$ at $t_{\alpha,\beta,\gamma,\delta,\psi}$ as shown in the top plot, according to the timing in Fig. 3. Meanwhile, the pseudo-measurements of $\omega(t)$ are shown in the middle plot. In addition, in the bottom of Fig. 4, the input signal $r(t)$ is shown. It can be observed that the simulation scenario is set up such that a probing experiment is performed according to the timings in Fig. 3, regardless if a new control design is needed or not. This is done to ease the simulation process. In this simulation, the PSS controller is parametrized with two constants k_w and t_w:

$$K(s) = k_w \left[(t_w)/(1 + t_w s)\right]. \tag{7}$$

The original controller K_0 has parameters $k_{w,0}$ =5.0 and $t_{w,0}$ =5.0 s As will become clear later, K_0 is in operation until t_{K_1} =20.0 min., when a newly designed controller $K_{new,1} = K_1$ will be applied and kept through the reminder of the simulation. The probing signal is still applied, although it is not required (see later). This will indeed serve to assess the performance of the new controller in more detail.

3.2 Illustration of Procedure 1

Applying Procedure 1 as described Section 2.2 to the ambient data collected from $\omega[n]$ between t =[7.5,12.5] min., $\hat{H}$ was estimated as shown in Fig. 5 in (blue) compared to the true H_0 (red). It was obtained using an ARMA model structure from MATLAB's System Identification Toolbox by setting the `armax` function with `na=nc=8`.

$\hat{H}$ gives a fit of 87.74%. This fit is quite good considering the low model order of 8 used as compared to the higher order of H_0 which contains 52 states. Using a higher order model does not give better results, as there are several modes that are not observable by $\omega(t)$ in any case (see Vanfretti and Chow (2010)). Procedure 1 also gives:

$$\xi_{min}(\hat{H}) = 0.0564 \text{ and } \mathcal{I}_{\hat{H}} = \{0.0,\ 0.0876\}. \tag{8}$$

Note that the true value is ξ_{true}=0.0591 and what it is obtained from (8) is only 4.5 % lower, while the true value is contained within the upper bound of $\mathcal{I}_{\hat{H}}$. This indicates that the damping is insufficient for a ξ_{req}=15%. This assessment gives the confidence of applying the next step of the methodology, as discussed below.

3.3 Illustration of Procedure 2

Having found that the damping is not adequate, Procedure 2 is applied as described in Section 2.3. To this end the probing signal r (which is here a multisine) is applied and data for $\omega[n]$ and $r[n]$ from t =[12.5,17.5] min are collected. To estimate $\hat{T}$ using this data, a Box-Jenkins model with parameters `nb=nc=nd=nf=6` and `nk=0` is selected, achieving a fit of 89.84%.

This yields $\hat{T}$ shown in Fig. 6 in red (with its uncertainty shaded in red). The figure also compares the true T_0

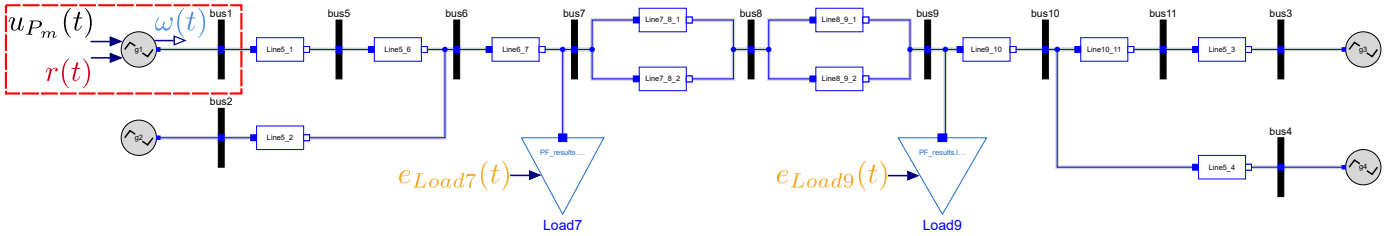

Fig. 2. Two-Area Four-Machine Klein-Rogers-Kundur Power System Model

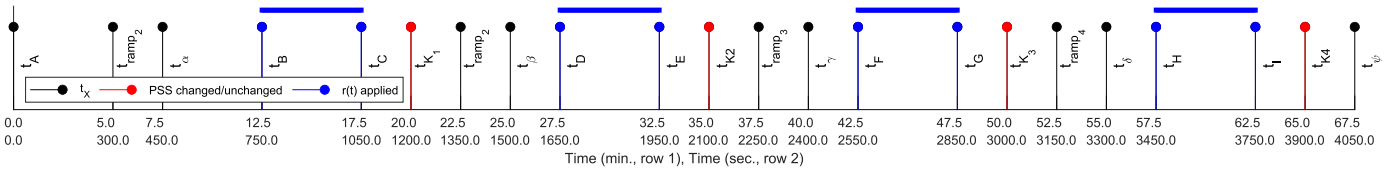

Fig. 3. Sketch of Simulation Scenarios with Multiple OPs, Probing Signals and new PSS Design Application

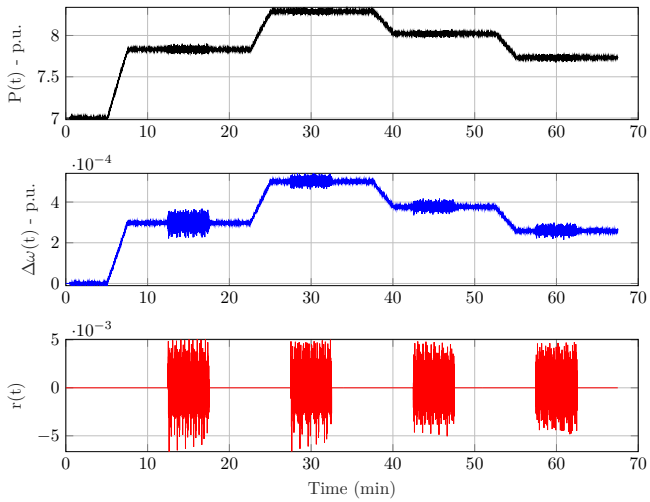

Fig. 4. Simulation of the Model in Fig. 2 under Ambient Conditions and Multiple Operating Points

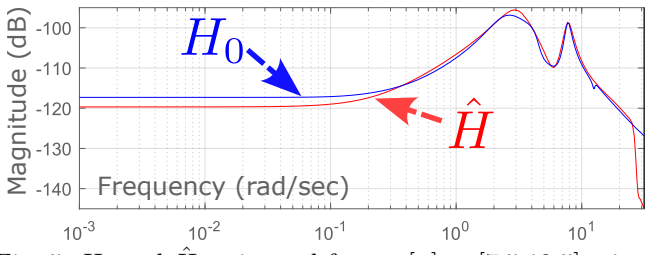

Fig. 5. H_0 and $\hat{H}$ estimated from $\omega[n]$ t=[7.5,12.5] min.

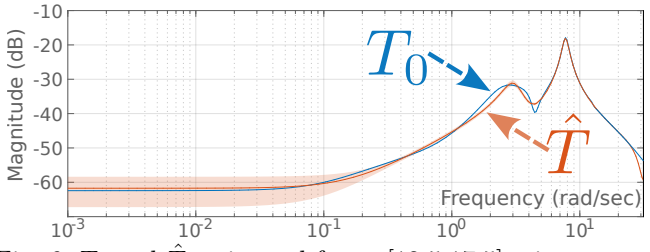

Fig. 6. T_0 and $\hat{T}$ estimated for t=[12.5,17.5] min

(obtained from the linearized model) with $\hat{T}$. We can note that at the dominant oscillation's frequency, 7.7 rad/s (≈1.22 Hz), the estimated model has high-accuracy and low uncertainty. In addition, the estimated model $\hat{G}$ obtained using (6) using $\hat{T}$ and K_0 is shown in Fig. 7 (in red) and compared with the true G_0 (in blue). It can be observed in this figure how $\hat{G}$ closely matches G_0 (especially for the mode at 7.7 rad/s).

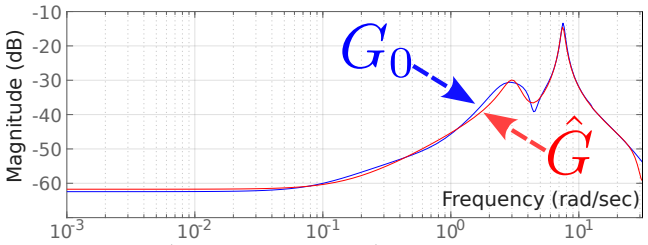

Fig. 7. G_0 and $\hat{G}$ estimated from $\hat{T}$ and K_0 for t=[12.5,17.5] min

Next, from $\hat{T}$ we compute:

$$\xi_{min}(\hat{T}) = 0.0615 \text{ and } \mathcal{I}_{\hat{T}} = \{0.0604,\ 0.0628\}, \quad (9)$$

noting that $\mathcal{I}_{\hat{T}}$ has narrower uncertainty than the one obtained with blind identification ($\mathcal{I}_{\hat{H}}$), with the lower bound of 0.0604 being only 2.2% higher than the true damping value ξ_{true}= 0.0591. Having confirmed that $\{\xi_{min}(\hat{T}) \wedge \mathcal{I}_{\hat{T}}\} < \xi_{\text{req}}$, we now redesign the PSS using Procedure 3.

3.4 Illustration of Procedure 3

Using $\hat{G}$ identified in Procedure 2 (see Fig. 7), we have a good quality model to perform PSS redesign using Procedure 3 as described in Section 2.4. Applying the method proposed in Bombois and Vanfretti (2023), gives a new controller K_1 with parameters $k_{w,1}$=49.6273 and $t_{w,1}$=0.3801 s.

Before applying the new controller, we compute:

$$\xi_{min}(K_1, \hat{G}) = 0.3230 \ \& \ \mathcal{I}_{new,1} = \{0.2741, 0.3305\}, \quad (10)$$

which are larger than ξ_{req}=15.00%, and consequently, it is decided to apply the new PSS design at t=20 min., as it provides a damping of 32.30% with bounds larger than ξ_{req}.

The new controller has thus high damping ability when applied to the model $\hat{G}$. This is also the case when this controller is applied to the true G_0. Indeed, ξ_{min} (K_1, G_0) = 26%. Note that this value is slightly lower than the lower bound in $\mathcal{I}_{new,1}$ (see (10)). This small discrepancy can be

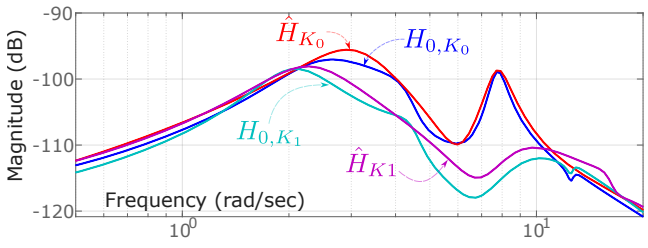

Fig. 8. Assessment of the application of $K_{new} = K_1$

explained by the fact that the uncertainty intervals are derived based-on a full-order model assumption, which is not fully satisfied in our case.

3.5 Redesigned Controller Performance Analysis

3.5.1 Verification using Blind Identification. We replace K_0 by the new controller K_1. While this controller is operating under ambient conditions, it is possible to use ambient data to verify the performance of K_1, that is, to verify that $\xi_{min}(K_1, G_0)$ is satisfactory. This can be achieved by applying Procedure 1 again with data from t=[1200-1350]. To this end, we use an ARMA model with `na=nc=8` to estimate $\hat{H}_{K1}$ using blind identification; this gives $\hat{H}_{K1}$ shown in Fig. 8 in magenta, compared to H_{0,K_1} (in cyan) and for contrast also to $\hat{H}_{0,K_0}$ (in red) and to H_{0,K_0} (in blue) (which are also shown in Fig. 5). Comparing $\hat{H}_{0,K_0}$ (red) with $\hat{H}_{K_1}$ (magenta) reveals that the designed controller has effectively removed the peak at 7.7 rad/s (≈1.22 Hz) by providing substantial damping.

As can be observed in Fig. 8, the mode at ω =7.7 rad/s (which results from interactions between the power plants `g1` and `g2`) is no longer the one with the smallest damping. The mode with the smallest damping is a lower frequency mode at ≈2.4 rad/s. This is the so-called inter-area mode (see Klein et al (1991)). The model $\hat{H}_{K_1}$ can be used to see that this mode has a damping equal to 24.74% i.e., $\xi_{min}(\hat{H}_{K_1}) = 24.74\%$. Therefore, the monitoring procedure confirms that K_1 is very likely to have sufficient damping ability. Note also that this estimate of the minimal damping is very close to the minimal damping of H_{0,K_1} since $\xi_{min}(H_{0,K_1}) = 25.91\%$. This is precisely what was observed in Section 3.4, i.e., $\xi_{min}(K_1, G_0)$ =26%.

Remark. Besides the two modes discussed above, the power network described in Fig. 2 also has an additional mode. This third mode results from interactions between the power plants `g3` and `g4` i.e., plants located at the other end of the power network (Klein et al, 1991). This mode is almost unobservable at the location of the power plant `g1` (see the tiny peak that appears at ≈ 13.2 rad/s in the frequency response of both H_{0,K_0} (blue) and H_{0,K_1} (cyan)). Since it does not influence the dynamics that can be observed at `g1`, this third mode cannot be identified (it therefore does not appear in $\hat{H}_{K_0}$ and $\hat{H}_{K_1}$). This is not a problem because the objective of the PSS controller at `g1` is to only damp the two observable modes at `g1`. The third mode has, e.g., to be addressed by another PSS controller located at `g3` or at `g4`. For all these reasons, we have not considered this third mode when computing $\xi_{min}(K_1, G_0)$ and we will do so in the sequel.

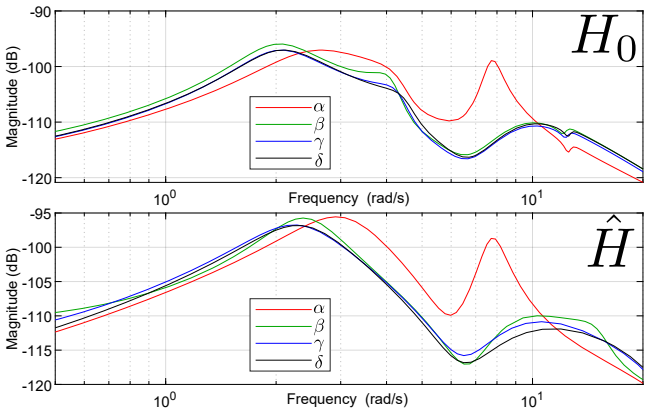

Fig. 9. H_0 and $\hat{H}$ at Multiple Operating Points

3.5.2 Procedure 1 at Multiple Operating Points. In the previous subsection, our monitoring procedure has thus confirmed that K_1 has sufficient damping ability at the operating point α. Let us now test our monitoring procedure when the system with the new PSS controller K_1 is operating under ambient conditions at other operating points (OPs) (i.e., with a different G_0). In Fig. 4, this situation is simulated during the intervals $t_{\beta-D}$=[25.0, 27.5], $t_{\gamma-F}$=[40.0, 42.5] and $t_{\delta-H}$=[55.0, 57.5] minutes, corresponding to the dispatch levels of $P_{\beta,\gamma,\delta} \approx [8.29, 8.02, 7.73]$ p.u.

At these three operating points, we apply Procedure 1, similar to what was done in Section 3.2. The estimated $\hat{H}$ and the true system H_0 corresponding to these three operating points are shown in Fig. 9. To show the improvement when replacing K_0 by K_1, we also represent in this figure the H_0 and $\hat{H}$ for OP α when K_0 was the PSS controller (i.e., the H_0 and $\hat{H}$ represented in Fig. 5).

Observing Figure 9, it is clear that the new PSS controller K_1, which performs well at OP α (see Fig. 8), also performs well at the operating points β, γ and δ.

In fact, similar to what was observed in Fig. 8 for OP α, the sharp peak at ≈7.7 rad/s when K_0 is used (red curve in Fig. 9) disappears in the TFs H_0 obtained with K_1 at the operating points β, γ and δ. Furthermore, as was also observed for OP α in the previous subsection, the mode corresponding to the minimum damping with the new controller K_1 is the one located at ≈2 rad/s. Figure 9 also shows that this mode is well damped in OPs β, γ and δ.

Let us now see whether our monitoring procedure (Procedure 1) allows us to confirm this result. Using the identified TFs $\hat{H}$ at the OPs β, γ and δ, we can estimate the minimal damping $\xi_{min}(H_0)$ achieved by K_1 at these operating points by $\xi_{min}(\hat{H})$. Since $\xi_{min}(\hat{H}) \approx 25\%$ for the three operating points, our monitoring procedure would rightly conclude that K_1 achieves sufficient damping at these operating points.

Remark. The robustness of the controller K_1 is noticeable. Note in fact that the power system operates at a much larger dispatch at OP β than at OP α (OP at which K_1 has been designed).

3.5.3 Procedure 2 at Multiple Operating Points. In the previous subsection, the monitoring procedure (Proce-

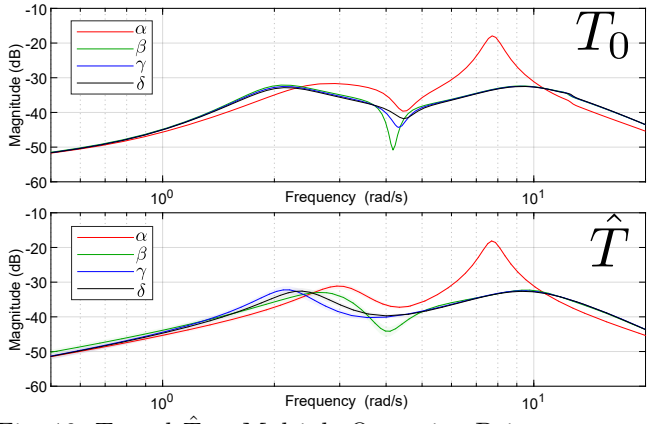

Fig. 10. T_0 and $\hat{T}$ at Multiple Operating Points

dure 1) has indicated that the performance of K_1 is also satisfactory in the OPs β, γ and δ. According to the methodology proposed in Section 2, probing-based identification will therefore normally not be applied. However, for the sake of completion, we have decided to perform this probing-based identification (Procedure 2). Therefore, we collect data during the probing periods t_{D-E}, t_{F-G} and t_{H-1} and, similarly to Section 3.3, we apply the second procedure to these time periods. The results are presented in Fig. 10 in a similar manner as in Fig. 9, replacing H_0 (resp. $\hat{H}$) by T_0 (resp. $\hat{T}$). The red curve (OP α) corresponds thus to the closed-loop TF T_0 with the original controller K_0

It is clear that the observation of the different graphs of T_0 in Fig. 10 leads to the same conclusions as the observation of the different graphs of H_0 in Figure 9 i.e., that K_1 is a satisfactory controller.

Note also that the models $\hat{T}$ remain a good representation of T_0 (see Fig. 10).

4. CONCLUSION

This paper showed that, using both blind and probing-based identification techniques, it is possible to monitor the dominant oscillatory modes of a power plant operating under ambient conditions and at multiple dispatch points. Moreover, it was shown that by performing probing-based identification, a high-quality data-driven model can be obtained to perform PSS redesign, without the need of any conventional simulation models. In addition, it is shown that such a design can be successful in maintaining adequate damping at multiple OPs.

REFERENCES

L. Ljung, *System Identification: Theory for the User, 2nd Edition*. Englewood Cliffs, NJ: Prentice-Hall, 1999.

X. Bombois and L. Vanfretti, "Performance monitoring and redesign of power system stabilizers based on system identification techniques," Sustainable Energy, Grids and Networks, Volume 38, 2024, 101278, ISSN 2352-4677, `https://doi.org/10.1016/j.segan.2024.101278`. Pre-print available online: `https://hal.archives-ouvertes.fr/hal-03708303`

X. Bombois, "Optimal identification experiment design software". Research Report, Laboratorie Ampere. Available online: `https://hal.science/hal-03175027`

M. A. Gelbart, J. Snoek, and R. P. Adams, "Bayesian optimization with unknown constraints," *arXiv preprint arXiv:1403.5607*, 2014.

M. Klein, G. J. Rogers and P. Kundur, "A fundamental study of inter-area oscillations in power systems," in IEEE Transactions on Power Systems, vol. 6, no. 3, pp. 914-921, Aug. 1991.

M. de Castro et al "Version [OpenIPSL 2.0.0] - [iTesla Power Systems Library (iPSL): A Modelica library for phasor time-domain simulations]", SoftwareX, Volume 21, 2023, ISSN 2352-7110.

F. Milano, *Power System Modeling and Scripting*. Springer-Verlag, Berlin, Heidelberg, 2010.

"PSS(®)E 34.2.0 Model Library," Siemens PTI, Schenectady, NY (2017).

M. Baur, M. Otter, and B. Thiele, "Modelica Libraries for Linear Control Systems," in *7th International Modelica Conference*, ser. 43. Proc., 2009, pp. 593–602.

D. Bruck et al, "Dymola for Multi-Engineering Modeling and Simulation," 2nd International Modelica Conference, Oberpfaffenhofen, Germany, 2002, pp. 55-1-55-8.

A. Klöckner, A. Knoblach and A. Heckmann, "How to shape noise spectra for continuous system simulation," in Mathematical and Computer Modelling of Dynamical Systems, vol. 23, no. 3, pp. 284-300, 2017.

T. Xu et al, "Application of Large-Scale Synthetic Power System Models for Energy Economic Studies," in Proc. 50th Hawaii Intl. Conf. on Sys. Sciences, 2017, pp. 3123 – 3129.

G. Rogers, "The effect of power system stabilizers on system performance," in Proc. 1999 IEEE Power Eng. Soc. Summer Meeting (Cat. No.99CH36364), Edmonton, AB, Canada, 1999, pp. 110-115 vol.1.

E. Rebello, L. Vanfretti and M. S. Almas, "Experimental Testing of a Real-Time Implementation of a PMU-Based Wide-Area Damping Control System," in IEEE Access, vol. 8, pp. 25800-25810, 2020.

ENTSO-E Sub-Group System Dynamics and Protection, "Analysis of CE Inter-Area Oscillations of 1st December 2016," *ENTSO-E*, 2017, Available online: https://tinyurl.com/ENTSOE2016, Accessed: October 5, 2022.

ENTSO-E, "Oscillation Event 03.12.2017," 2018, Available online: https://tinyurl.com/ENTSOE2017, Accessed: October 5, 2023.

C. Mishra et al, "Analysis of STATCOM Oscillations using Ambient Synchrophasor Data in Dominion Energy," 2022 IEEE PES ISGT Conference, New Orleans, LA, USA, 2022, pp. 1-5.

V. S. Peric, X. Bombois and L. Vanfretti, "Optimal Signal Selection for Power System Ambient Mode Estimation Using a Prediction Error Criterion," in IEEE Trans. on Power Systems, vol. 31, no. 4, pp. 2621-2633, July 2016.

L. Vanfretti and J. H. Chow, "Analysis of power system oscillations for developing synchrophasor data applications," 2010 IREP Symposium Bulk Power System Dynamics and Control - VIII, Rio de Janeiro, Brazil, 2010, pp. 1-17, doi: 10.1109/IREP.2010.5563289.